Electronic structure of (Zn,Cd)(S,Se)-based polytype superlattices

Z. Z. Bandić* and Z. Ikonić
Division of Physical Electronics, Faculty of Electrical Engineering, University of Belgrade, Bulevar Revolucije 73, 11000 Beograd, Yugoslavia
(Received 26 September 1994)

The local empirical pseudopotential theory in the *S*-matrix implementation was used to study the structure of (Zn,Cd)(S,Se) polytypes considered as natural heterocrystalline superlattices. Hexagonal polytype superlattices of (Zn,Cd)(S,Se) are predicted to be characterized by direct band gaps and have minibands derived from evanescent bulk states, which collapse into the heterocrystalline interface bound states or resonances above the valence-band edge. There is a linear relationship between various band gaps and hexagonality *h*. The superlattice wave function is strongly localized in the cubic portions of superlattice unit cell.

I. INTRODUCTION

Polytype (heterocrystalline) superlattices, along with recently proposed twinning superlattices,[1] present a type of superlattices in which the coherent scattering of electrons at interfaces and the formation of superlattice states happens in a different way than with conventional superlattices, based on periodic changes of either composition or doping patterns. Periodic variations in material composition and the periodic electrostatic potential (in the case of doping superlattices) are not the only way to introduce electron scattering in semiconductors. There are at least two different ways to make a single semiconductor material behave as an inhomogeneous structure; by introducing periodic changes in the crystal orientation or crystal structure. Periodically arranged twin stacking faults or 180° twist boundaries are the scattering centers for electrons in the case of twinning superlattices (they may be viewed as purposely built-in periodic reversals of atomic plane stacking sequences, for example in the [111] direction of diamond-type and zinc-blende-type semiconductors). On the other hand, heterocrystalline superlattices consist of two different types of crystal structure, cubic and hexagonal (or zinc blende and wurtzite) of the same material, periodically repeated in the [111] direction of the cubic and [0001] direction of the hexagonal lattice. A common property of both heterocrystalline and twinning superlattices is the lack of stress and/or dangling bonds, because the interface between two crystal structures or two crystal orientations is almost perfectly lattice matched.

The polytypes of chalcogenides (Zn, Cd) (S, Se) can spontaneously appear in nature,[2] because the formation energies of the two constituent crystal phases differ by a very small amount. It is thus possible to consider them as natural homomaterial heterocrystalline superlattices. Although there has been no clear report on epitaxial growth of heterocrystalline superlattices, more than 185 hexagonal and rhombohedral polytypes of ZnS have been reported, mostly in synthetically grown crystals.[2] Unfortunately, laboratory-grown polytypes usually occur in the form of needles or elongated plates, with the *c* axis, along which the polytype periodicity varies, lying along the length of the plate.

Polytype superlattices were studied some time ago in the work of Dubrovskii and co-workers within the framework of the relatively simple Kronig-Penney model.[3,4] They have been considered as possible artificial superlattice structures by Ren and Dow,[5] where a tight-binding supercell calculation of their electronic properties was done, on the example of CdS. Interest in this field was recently renewed, and more sophisticated methods were used to calculate energy differences between zinc-blende and wurtzite crystal phases for all simple binary superconductors,[6] structural and electronic properties of SiC polytypes,[7,8] electronic structure of Si and ZnS heterocrystalline superlattices,[9,10] band offsets and their chemical trend for heterocrystalline junctions of various semiconductors,[11] etc.

In addition to a purely theoretical motivation to study polytipism and polytype (heterocrystalline) superlattices, the reasons for the recently renewed interest in these structures lie in the great potential of wide-band-gap semiconductors to high-temperature and electro-optical (ultraviolet and near-visible range) applications. Wide band gaps are consequences of the covalent bonding which guarantee good thermomechanical properties, with SiC being the best example. On the other hand, the bonds in chalcogenides are believed to be partially covalent and partially ionic.[2] This implies that (Zn, Cd) (S, Se) crystals are not as good in their thermomechanical properties as SiC. However, there still exists a wide range of standard electro-optical applications: CdS, CdS_xSe_{1-x}, and ZnSe are important materials for use in light-emitting diodes (LED's) and lasers in green, red, and blue ranges of the visible spectrum respectively;[12,13] CdS is interesting for solar cells;[14] and *n*-doped CdSe is found to be a promising material for heterojunction wide-band-gap light emitters.[15]

In this paper we used the empirical pseudopotential layer method in the *S*-matrix implementation[16] to study the electronic properties of chalcogenides (Zn,Cd) (S,Se)-based hexagonal polytypes, considered heterocrystalline superlattices (the term hexagonal here refers to the type

0163-1829/95/51(15)/9806(7)/$06.00

of the superlattice unit cell). These polytypes are the only semiconductor materials, other than SiC-based ones, that are at present known to exist under normal conditions. The nature of the highest valence and the lowest conduction minibands, or more precisely, the superlattice state wave function composition has also been determined.

II. METHOD AND THEORETICAL CONSIDERATIONS

Direct-band-gap chalcogenides semiconductors (Zn,Cd) (S,Se) spontaneously show polytipism. The two crystalline phases, the face-centered-cubic (or zinc-blende) and hexagonal-close-packed (or wurtzite) may coexist, because of the small difference of their internal energies (of order 1–3 meV/atom),[6] and rather subtle structural differences, which manifest as different layer stackings of the cubic (111) or hexagonal (0001) planes. The stacking sequences of cubic (fcc) and hexagonal (hcp) materials are $ABCABC\ldots$ and $ABAB\ldots$, while $ABCB\ldots$, $ABCACB\ldots$, $ABCABACB\ldots$, and $ABCABCBACB\ldots$ are the sequences for $4H$, $6H$, $8H$, and $10H$ hexagonal polytypes, respectively. In this notation A, B, and C denote the two basis atoms of the primitive unit cell. The system (polytype) is considered a periodic repetition of a heterocrystalline superlattice unit cell along the growth direction. One hexagonal polytype superlattice unit cell consists of three layers, two cubic (one of which is rotated by 180°) and one wurtzite layer. For example, the $6H$ polytype superlattice unit cell, as shown in Fig. 1, contains one wurtzite monolayer and two zinc-blende layers, both of which have two atomic monolayers.

The method used in our calculations is the local empirical pseudopotential theory, implemented via the S-matrix method,[16–19] adapted for heterocrystalline superlattices. The complex band structure and eigenfunctions of both the propagating and evanescent states of constitutive fcc and hcp portions in the superlattice unit cell are calculated in the growth direction using the local empirical pseudopotential theory. The superlattice wave function in each crystal phase is expressed as a linear combination of the corresponding bulk states. These wave functions and their derivatives at a given energy E and parallel wave vector $k_{\parallel}$ are matched at the interfaces between the two phases using the S-matrix approach, which guarantees high stability against the evanescent states.[17] After propagation along the full superlattice period, the T matrix is reconstructed from the final S matrix,[17] the Bloch-like theorem is applied, the eigenequation is solved, and the polytype superlattice miniband structure is calculated. The coordinate origins in the zinc-blende and wurtzite real-space unit cells are chosen so that the position of each basis atom of one type (for example Zn) goes into the position on an atom of the second type (for example S) upon spatial inversion. With this choice, structure form factors S^S and S^A are real.[20] In order to match correct values of wave functions and their derivatives, interface planes are placed exactly in between two atoms, as shown in Fig. 1. This choice is influenced by the fact that the pseudopotential wave function contains no characteristic atomic oscillations in the vicinity of the ion, but outside the core region it is almost the same as the real plane-wave-like wave function.

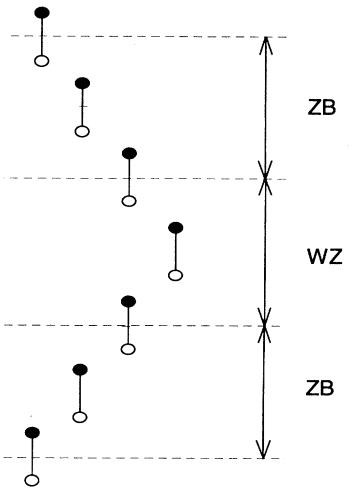

FIG. 1. The $6H$ polytype superlattice unit cell ($ABCACB$) contains one wurtzite (WZ) and two zinc-blende (ZB) layers. Interface planes are placed exactly in between two atoms.

There is another interesting point concerning the plane of wave-function matching, first noted by Ren and Dow,[5] stemming from the fact that the position of the zinc-blende–wurtzite interface plane is not unambiguous, unlike the case for conventional superlattices. This does not lead to any ambiguity in calculating the miniband structure, provided some care is taken when writing the supercell tight-binding Hamiltonian, as shown in Ref. 5. We shall demonstrate here that no ambiguity arises in our bulk-based (not supercell) empirical pseudopotential calculation. Take the $4H$ polytype, for example (or 2×1 in the notation of Ref. 5), having the stacking sequence $\ldots ABCBABCBA\ldots$ of atomic bilayers. One may now choose the superlattice period as enclosed in square brackets, starting at the position A:

$$\ldots ABCB[(AB)_z|(CB)_w]ABCB\ldots ,$$

where the subscripts denote the crystalline structure of atomic bilayers, the contents of the parentheses are assigned in accordance to their nearest neighbors, and the bar denotes the position of the interface plane. Alternatively, shifting the origin of the superlattice period by one to the right, i.e., starting from the position B, the superlattice period would be

$$\ldots BCBA[(BC)_w|(BA)_z]BCBA\ldots ,$$

and the interface plane is clearly displaced from the former case. However, the structure of the superlattice period in the latter case, if read in the reverse (i.e., $-z$) direction, coincides with the one in the former case. Since the miniband structure does not depend on which direction along the [111] axis is denoted as positive or negative, there is no ambiguity in the calculation: once the superlattice period is chosen, its portions having zinc-blende or wurtzite crystalline structure are uniquely determined.

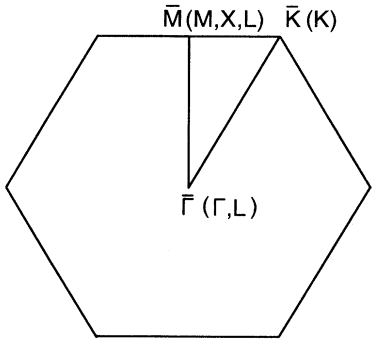

FIG. 2. The zinc-blende–wurtzite interface Brillouin zone, with mapping of some important bulk Brillouin-zone points.

The first Brillouin zone of the zinc-blende crystal phase is the well-known truncated octahedron, while in the case of wurtzite it is the simple hexagonal Brillouin zone. The interface Brillouin zone, with mapping of some important bulk Brillouin zone points, is shown in Fig. 2. The points Γ, M, and K of the hexagonal Brillouin zone for wurtzite are mapped onto the $\bar{\Gamma}$, $\bar{M}$, and $\bar{K}$ points of the interface Brillouin zone, respectively. In the case of the zinc-blende crystal phase, all six equivalent X points of the first Brillouin zone are projected onto six distinct $\bar{M}$ points. On the other hand, two of the eight equivalent L points along with Γ are projected onto $\bar{\Gamma}$, while other six are projected onto $\bar{M}$. Various states in the superlattice Brillouin zone are accessed by presetting an appropriate value of parallel wave vector $k_{\parallel}$ (the in-plane projection of the electron wave vector) within the interface Brillouin zone, and the superlattice wave vector (k_{SL}) comes out of the calculation, thus giving the miniband structure.

It is important to point out that this method does not belong to the class of *ab initio* supercells method, such as first-principles pseudopotentials within the local-density approximation.[7,9–11] As the superlattice period grows large, they become computationally very demanding, and generally produce unreliable band gaps. On the other hand, the S-matrix layer method guarantee that both short as well as long superlattice periods may be treated in essentially the same way, without encountering any computational problems, while empirical pseudopotentials provide a realistic band structure. Other methods have also been used to study polytype superlattices, especially for SiC. Energy-band structure and optical properties of both hexagonal and rhombohedral SiC polytype superlattices were successfully studied within the simple Kronig-Penney model in the work of Dubrovskii and coworkers.[3,4] It seems that the effective-mass-type calculation alone is not sufficient to explain all electronic properties of (Zn,Cd) (S,Se) polytype superlattices, since the two crystal phases have very similar values of band gaps and small band offsets. SiC polytypes were also studied by the empirical pseudopotential method in the work of Backes, Bobbert, and Haeringen[8] in a way similar to that applied to twinning superlattices.[1,19] Our model is obviously different, since they consider a superlattice unit cell consisting of pure cubic segments which differ only in size and crystal orientation, while we are interested in revealing those properties of polytype superlattices arising from interface scattering and/or band mixing at wurtzite–zinc-blende boundaries. Furthermore, the percentage of the total $|\Psi_{\mathrm{SL}}|^2$ accumulated in cubic and hexagonal portions of the unit cell can also be calculated to qualitatively indicate the degree of charge transfer across the heterocrystalline interfaces.

III. RESULTS AND DISCUSSION

Numerical calculations for ZnS and Cd(S,Se) polytype superlattices were performed using the Bergstresser-Cohen set of empirical pseudopotential form factors,[20,21] since they give reasonably good values of various band gaps in both crystalline phases of the materials. In the case of hexagonal ZnSe, our proposal for the atomic form factors for the corresponding values of squares of the wurtzite reciprocal-lattice vectors is listed in Table I. The symmetric form factors are initially obtained as the average of the symmetric form factors for hexagonal ZnS and CdS, since the lattice constant of ZnSe is found almost exactly between the lattice constants of ZnS and CdS. The antisymmetric form factors are calculated in a way similar to Bloom,[22] using the zinc form factors from Animalu and Heine[23] and Harrison.[24] After this calculation both symmetric and antisymmetric form factors were slightly readjusted to fit the values of the form factors for cubic ZnSe from Ref. 21.

A complex band-structure calculation and interface matching have been done with 19 two-dimensional plane waves, which correspond to a set of 59 and 135 three-dimensional vectors for cubic and hexagonal reciprocal lattices, respectively. Because of the neglect of charge transfer in our model, band offsets generally do not quite agree with experimentally established values. That is why it was sometimes necessary to introduce an external parameter—a downward or upward shift of the band structure of one constituent of the superlattice—as in

TABLE I. Atomic form factors for hexagonal (wurtzite) ZnSe in Ry.

$\lvert\mathbf{G}\rvert^2$	V^S	V^A
0		
3/4		
2-2/3	− 0.25	
3	− 0.23	0.18
3-5/12	−0.20	0.15
5-2/3	−0.05	0.09
6-3/4		
8	0.01	
8-3/4		
9-5/12	0.05	0.03
10-2/3	0.06	
11	0.06	0.03
11-5/12	0.06	0.03
12		0.03
13-2/3	0.03	0.01
14-2/3		0.01
14-3/4		

Ref. 17. Since we are not presently aware of any experimental data for band offsets at the wurtzite–zinc-blende heterocrystalline interfaces, Murayama and Nakayama's local-density approximation (LDA) calculations of the band offsets at various heterocrystalline semiconductor interfaces, including (Zn,Cd) (S,Se), have been consulted.[9–11] It is interesting that our empirical pseudopotential calculation, except in the case of CdSe, gives values for band discontinuities at the Γ point, ΔE_v and ΔE_c, which are in very good quantitative agreement with the values of Murayama and Nakayama obtained from first-principles pseudopotential calculations. This result confirms their thesis that charge transfer through heterocrystalline interfaces is very small, and that no dipole potential appears at the interface, so that the band offsets would be very small and determined only by the difference between original energy levels in wurtzite and zinc-blende crystal phases. In the case of CdSe, an external downward shift of the hexagonal CdSe band structure by $V_{\rm off}=0.08$ eV can adjust only the valence-band offset, leaving an incorrect value for the conduction-band offset, or vice versa. This disagreement is probably the consequence of an inadequate choice of atomic form factors, but we expect that all major physical effects and their trends should be revealed. The spin-orbit interaction is not taken into account. However, the atomic form factors used in this paper[20,21] are obtained to give band structures in good agreement with the experimental data, from which the spin-orbit coupling is artificially removed. Actually, the energy of a level, degenerate without the spin-orbit interaction, is taken as the average of its component levels, weighted over their degeneracies. Calculated energies at the points Γ, M, and X for both crystal phases of (Zn,Cd) (S,Se), along with band gaps and offsets, are listed in Table II. We should note that the layer method employed in this work tends to give slightly smaller band-gap values than the Hamiltonian matrix diagonalization method used by Cohen and Bergstresser.[20,21]

TABLE II. Energies at the symmetric points Γ, M, and X of the bulk Brillouin zones for both the hexagonal (wurtzite) and cubic (zinc-blende) crystal phases of (Zn,Cd) (S,Se). Band gaps and offsets are also displayed. All the energies are in eV, and are given as they came out of calculation, i.e., not measured from any significant reference point.

	ZnS	CdS	ZnSe	CdSe
ZB				
Γ_v	6.40	4.15	6.31	4.01
Γ_c	10.03	6.65	8.38	5.87
X_c	11.37	8.64	10.11	7.95
E_g	3.63	2.5	2.07	1.86
WZ				
Γ_v	6.43	4.18	6.34	4.04
Γ_c	10.09	6.72	8.47	5.87
M_c	11.45	9.15	10.22	8.41
E_g	3.66	2.54	2.13	1.83
Offsets				
ΔE_v	0.03	0.03	0.03	0.03
ΔE_c	0.06	0.07	0.09	0.00

The results of present calculations for (Zn,Cd) (S,Se) hexagonal polytypes are given in Table III, while Fig. 3 shows the energy miniband structure of ZnS polytypes. Calculations were performed for the $\bar{\Gamma}$ and $\bar{M}$ points of the interface Brillouin zone, since the low-energy part of the electronic structure is to be expected only near them. The first two allowed conductions minibands along with the first valence miniband are calculated at the $\bar{\Gamma}$ point, while the first conduction miniband is calculated at the $\bar{M}$ point. Values of the direct band gap and the lowest indirect band gap are also given in Table III. Polytype superlattices based on (Zn,Cd) (S,Se) are obviously direct-band-gap materials. This was to be expected since the lowest indirect band gap in both crystal phases is much larger than the direct one, so the band mixing can hardly influence the character of the band gap. We have also calculated the composition of the superlattice wave function normalized to 100% in the superlattice period. The notation we use in Table III and Fig. 3 is as follows. $\bar{M}_c$:(c_1/c_2) means that c_1 percent of the total $\int|\Psi_{\rm SL}|^2dz$ is accumulated in zinc-blende layers, and c_2 in wurtzite layers, while the superlattice state is formed by the X bulk state of cubic and M bulk state of hexagonal crystal phases (both are projected onto the $\bar{M}$ point of the interface Brillouin zone). By inspecting the data in Table III we see that even in the case of $4H$ polytypes, where the percentage of the hexagonal close packing is $h=50\%$, superlattice states are dominantly localized in zinc-blende layers. This tendency becomes more noticeable with lowering of hexagonality h, and for $10H$ polytypes more than 80% of the total superlattice wave function is confined in cubic portions of the superlattice period for both conduction- and valence-band states. This is not in accordance with the quantum-well–barrier picture, which predicts holes to be localized in higher-energy wurtzite layers. Also, the quantum-well–barrier model, which is essentially the effective-mass-type calculation, cannot explain the fact that first valence minibands in all the polytype superlattices considered in this work are formed entirely from the evanescent bulk states. In addition, the bottom of the first conduction miniband at $\bar{\Gamma}$ and $\bar{M}$, for some polytypes (see Tables II and III), is partly below the bulk conduction-band edge of the cubic crystal phase. This feature has already been observed in the case of Si stacking fault systems,[25] where bound states are found 0.1 eV above the top of the valence band, and also in the case of twinning superlattices, where minibands formed entirely from evanescent bulk states are found below the bottom of the conduction band at the $\bar{\Gamma}$ point. For $4H$ polytypes we have calculated the top of the highest valence miniband at the $\bar{\Gamma}$ point to be at $E_v+0.28$, $E_v+0.16$, $E_v+0.09$, and $E_v+0.15$ eV for ZnS, CdS, ZnSe, and CdSe, respectively, while the corresponding bandwidths are 0.28, 0.15, 0.09, and 0.15 eV (E_v is the top of the valence band in the hexagonal crystal phase). As the superlattice period increases, these minibands collapse into single wurtzite–zinc-blende interface bound states (or resonance) from which they actu-

TABLE III. Allowed miniband energies and band gaps in (Zn,Cd) (S, Se)-based hexagonal polytype superlattices $4H$, $6H$, $8H$, and $10H$. Values of the first or first two miniband edges, separated by a dash, are given at $\bar{\Gamma}$ in the valence band ($\bar{\Gamma}_v$) and conduction band ($\bar{\Gamma}_c$), and at $\bar{M}$ in the conduction band (in the case of the valence band only the top of the second miniband is displayed). Numbers in parentheses denote the composition of the first miniband state (the notation is explained in the text). All the energies are in eV, and are given as they came out of the calculation, the reference point having no significance except that it is the same as in Table II, wherefrom we can see whether the miniband is in the allowed or forbidden band of the constituent bulk semiconductors.

	ZnS	CdS	ZnSe	CdSe
$4H$				
	...−6.41	...−4.12	...−6.31	...−4.02
$\bar{\Gamma}_v$	6.43−6.71	4.19−4.34	6.34−6.43	4.04−4.19
	(76/24)	(70/30)	(73/27)	(70/30)
	(67/33)	(67/33)	(68/32)	(67/33)
$\bar{\Gamma}_c$	10.0−10.77	6.65−7.34	8.36−9.17	5.85−6.54
	10.85−11.48	7.41−8.21	9.35−9.90	6.64−7.42
	(65/35)	(72/28)	(63/37)	(76/24)
$\bar{M}_c$	11.32−11.86	8.99−9.14	10.11−10.49	8.28−8.40
E_g^{dir}	3.29	2.31	1.93	1.66
E_g^{ind}	4.61	4.65	3.68	4.09
$6H$				
	...−6.41	...−4.12	...−6.32	...−4.02
$\bar{\Gamma}_v$	6.45−6.63	4.20−4.27	6.35−6.40	4.05−4.12
	(82/18)	(77/23)	(80/20)	(75/25)
	(80/20)	(80/20)	(81/19)	(80/20)
$\bar{\Gamma}_c$	10.01−10.42	6.65−7.00	8.37−8.83	5.86−6.20
	10.47−11.10	7.07−7.70	8.93−9.57	6.30−6.92
	(75/25)	(92/8)	(75/25)	(91/9)
$\bar{M}_c$	11.35−11.51	8.85−8.93	10.12−10.34	8.15−8.22
E_g^{dir}	3.38	2.38	1.97	1.74
E_g^{ind}	4.72	4.58	3.72	4.03
$8H$				
	...−6.42	...−4.14	...−6.33	...−4.03
$\bar{\Gamma}_v$	6.49−6.59	4.21−4.25	6.36−6.39	4.06−4.09
	(83/17)	(79/21)	(82/18)	(77/23)
	(85/15)	(86/14)	(86/14)	(85/15)
$\bar{\Gamma}_c$	10.02−10.26	6.66−6.85	8.37−8.65	5.86−6.06
	10.30−10.81	6.91−7.40	8.73−9.25	6.14−6.58
	(75/25)	(96/4)	(81/19)	(96/4)
$\bar{M}_c$	11.36−11.44	8.78−8.80	10.12−10.26	8.08−8.11
E_g^{dir}	3.43	2.41	1.98	1.77
E_g^{ind}	4.77	4.53	3.73	3.99
$10H$				
	...−6.42	...−4.14	...−6.33	...−4.03
$\bar{\Gamma}_v$	6.51−6.57	4.22−4.24	6.36−6.38	4.06−4.08
	(85/15)	(81/19)	(84/16)	(78/22)
	(88/12)	(89/11)	(89/11)	(88/12)
$\bar{\Gamma}_c$	10.02−10.17	6.66−6.78	8.37−8.56	5.86−5.99
	10.21−10.59	6.82−7.15	8.62−9.02	6.05−6.36
	(86/14)	(98/2)	(85/15)	(98/2)
$\bar{M}_c$	11.37−11.42	8.73−8.73	10.12−10.21	8.04−8.05
E_g^{dir}	3.45	2.42	1.99	1.78
E_g^{ind}	4.80	4.49	3.74	3.96

ally originate. This feature can be easily seen from Fig. 3, where the first valence miniband becomes more narrow with decreasing hexagonality. Consulting the data from Table III, we found interface bound states at approximately 0.24, 0.08, 0.06, and 0.06 eV above the valence-band edge (of the cubic crystal phase) for ZnS, CdS, ZnSe, and CdSe heterocrystalline interfaces. On the other hand, the bottom of the lowest conduction miniband at the $\bar{\Gamma}$ point is almost aligned with the bottom of the conduction band of the cubic phase, sometimes being 0.01 or 0.02 eV lower, except for CdS polytype superlattices. This indicates that folded zones interact weakly and

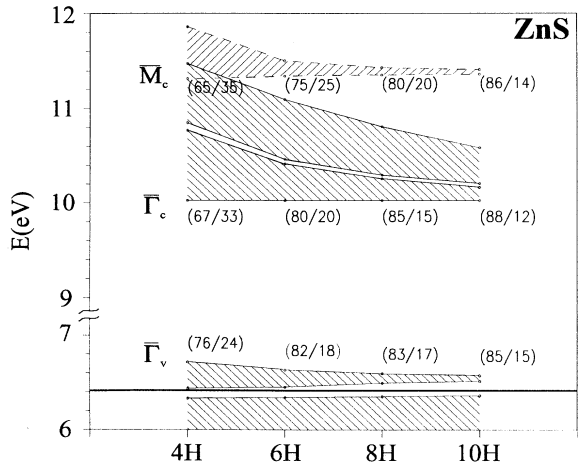

FIG. 3. The miniband energy structure of hexagonal ZnS-based superlattices, close to the $\bar{\Gamma}$ and $\bar{M}$ points. The first two allowed conduction minibands, along with the first valence miniband and the top of the second, are calculated at the $\bar{\Gamma}$ point (solid lines), while the first conduction miniband is calculated at the $\bar{M}$ point (dashed lines). The composition of the superlattice states at the top of the valence miniband at $\bar{\Gamma}$, and at the bottoms of the conduction minibands at $\bar{\Gamma}$ and $\bar{M}$ are also given. The notation is explained in the text. The first valence miniband is fully above the valence-band top of both crystal phases (thick horizontal line represent the top of the valence band of the cubic ZnS). It will obviously collapse into the wurtzite–zinc-blende heterocrystalline interface bound state as the superlattice period increases.

create interminiband separation in the 100-meV range, similar to that observed in conventional superlattices. In the case of Zn(S,Se) polytype superlattices, the bottom of the conduction miniband at the $\bar{M}$ point is aligned with the conduction band at the X point of the first Brillouin zone of the cubic crystal phase. This does not hold for Cd(S,Se) polytype superlattices, since there exists a larger energy separation between band edges at the X and M points of the bulk, thus making the crystal-type mismatch scattering at the interface less important than the common well-barrier scattering. That is why the trend of indirect band gap versus hexagonality h for Cd(S,Se) polytype superlattices is just the opposite to the trend for Zn(S,Se) polytype superlattices.

Energy-band-structure calculations show that strong linear relationships exist between both direct and lowest indirect band gaps and the hexagonality h in all polytype superlattices considered in this work. More precisely, the direct band gaps of all polytypes and the lowest indirect band gaps of Zn(S,Se) polytypes decrease with the hexagonality h, while the lowest indirect band gaps of Cd(S,Se) polytypes increase with hexagonality. The absolute value of the correlation coefficient $|r|$ is between 0.99 and 0.999 in all cases. Such linear relationships between the band gap and hexagonality were experimentally observed for SiC polytypes[26] and ZNS polytypes, which are also characterized by an analogous linear relationship between birefringence and hexagonality.[2] These linear relationships for SiC polytypes were successfully reproduced by Backes, Bobbert and van Haeringen[8] within the empirical pseudopotential scheme, but within a different model, as explained above. They also offer a simple but logical explanation within a Kronig-Penney-like model. Clearly, the one-dimensional Kronig-Penney model which was used in the work of Dubrovskii and coworkers[3,4] cannot explain these linear relationships for (Zn,Cd) (S,Se) polytypes. This is a consequence of the fact that the effective-mass-type calculation cannot account for superlattice states formed entirely from evanescent bulk states, and that precisely these minibands determine the values of band gaps. Similarly, these linear relationships were not revealed in Ren and Dow's supercell tight-binding calculations,[5] which is probably the consequence of the nearest-neighbor approximation.

IV. CONCLUSION

The electronic structure of chalcogenide (Zn,Cd) (S,Se) hexagonal polytypes considered as natural polytype (heterocrystalline) superlattices was analyzed within the local empirical pseudopotential framework. These materials are important since they have a wide range of electro-optical applications. The (Zn,Cd) (S,Se)-based hexagonal polytype superlattices are found to be direct-band-gap materials, with the values of the direct and the lowest indirect band gap linearly dependent on hexagonality h. They are also characterized by topmost valence minibands entirely formed from evanescent bulk states which originate from heterocrystalline interface bound states. The superlattice wave function is found to be localized in zinc-blende layers, for both valence- and conduction-band states, indicating low charge transfer through the heterocrystalline interface. None of these properties can be explained in terms of the effective-mass-type calculation. Finally, we may note that properties of the chalcogenide alloys polytypes, based on ternary and quaternary compounds within the (Zn,Cd) (S,Se) system, though not explicitly calculated here, may be estimated by interpolating between the results for the binary compound presented.

*Present address: Watson Laboratories of Applied Physics, California Institute of Technology, M/C 128-95, Pasadena, CA 91125.

[1]Z. Ikonić, G. P. Srivastava, and J. C. Inkson, Solid State Commun. **86**, 799 (1993).

[2]G. C. Trigunayat, Solid State Ion. **48**, 3 (1991); see also I. T. Steinberger and S. Mardix, in *International Conference on II-VI Semiconductor Compounds, 1967,* edited by D. G. Thomas (Benjamin, New York, 1967), p. 167.

[3]G. B. Dubrovskii and A. A. Lepneva, Fiz. Tverd. Tela Len-

ingrad **19**, 1252 (1977) [Sov. Phys. Solid State **19**, 729 (1977)].
[4]G. B. Dubrovskii and F. G. Pikus, Fiz. Tverd. Tela Leningrad **31**, 19 (1989) [Sov. Phys. Solid State **31**, 10 (1989)].
[5]S. Y. Ren and J. D. Dow, Phys. Rev. B **39**, 7796 (1989).
[6]C.-Y. Yeh, Z. W. Lu, S. Froyen, and A. Zunger, Phys. Rev. B **46**, 10 086 (1992).
[7]C. H. Park, B.-H. Cheong, K.-H. Lee, and K. J. Chang, Phys. Rev. B **49**, 4486 (1989).
[8]W. H. Backes, P. A. Bobbert, and W. van Haeringen, Phys. Rev. B **49**, 7564 (1994).
[9]M. Murayama and T. Nakayama, J. Phys. Soc. Jpn. **61**, 2419 (1992).
[10]M. Murayama and T. Nakayama, Superlatt. Microstruct. **12**, 215 (1992).
[11]M. Murayama and T. Nakayama, Phys. Rev. B **49**, 4710 (1994).
[12]S. Colak, B. J. Fitzpatrick, and R. N. Bhargava, J. Cryst. Growth **72**, 504 (1985).
[13]M. A. Haase, J. Qiu, J. M. DePuydt, and H. Cheng, Appl. Phys. Lett. **59**, 1272 (1991).
[14]T. L. Hench, J. A. Bragagnolo, J. E. Delgado, P. F. Leyman, and P. F. Motta, J. Vac. Sci. Technol. A **1**, 360 (1983).
[15]M. W. Wang, M. C. Phillips, J. F. Swenberg, E. T. Yu, J. O. McCaldin, and T. C. McGill, J. Appl. Phys. **73**, 4660 (1993).
[16]D. Y. K. Ko and J. C. Inkson, Phys. Rev. B **38**, 9945 (1988).
[17]Z. Ikonić, G. P. Srivastava, and J. C. Inkson, Phys. Rev. B **46**, 15 150 (1992).
[18]Z. Ikonić, G. P. Srivastava, and J. C. Inkson, Phys. Rev. B **49**, 10 749 (1994).
[19]Z. Ikonić, G. P. Srivastava, and J. C. Inkson, Phys. Rev. B **48**, 17 181 (1993).
[20]T. K. Bergstresser and M. L. Cohen, Phys. Rev. **164**, 1069 (1967)
[21]M. L. Cohen and T. K. Bergstresser, Phys. Rev. **141**, 789 (1966).
[22]S. Bloom, J. Phys. Chem. Solids **32**, 2027 (1971).
[23]A. O. E. Animalu and V. Heine, Philos. Mag. **12**, 1249 (1965).
[24]W. A. Harrison, *Pseudopotentials in the Theory of Metals* (Benjamin, New York, 1966).
[25]M. Y. Chou, M. L. Cohen, and S. G. Louie, Phys. Rev. B **32**, 7979 (1985).
[26]W. J. Choyke, D. R. Hamilton, and L. Patrick, Phys. Rev. **133**, 1163 (1964).